

Supplementary Materials:

## Solvent-Type-Dependent Polymorphism and Charge Transport in a Long Fused-Ring Organic Semiconductor

Jihua Chen,<sup>\*†</sup> Ming Shao,<sup>†</sup> Kai Xiao,<sup>†</sup> Adam J. Rondinone,<sup>†</sup> Yueh-Lin Loo,<sup>‡</sup> Paul R. C. Kent,<sup>†</sup> Bobby G. Sumpter,<sup>†</sup> Dawen Li,<sup>§</sup> Jong K. Keum,<sup>†</sup> Peter J. Diemer,<sup>⊥</sup> John E. Anthony<sup>¶</sup>, Oana D. Jurchescu,<sup>\*⊥</sup> Jingsong Huang<sup>†</sup>

### Simulation of UV-Vis Spectrum:

The bulk crystal structure was first optimized with density functional theory (DFT) using the Quantum Espresso 5.0 package.<sup>1</sup> Only the atoms in the triclinic unit cell were relaxed while the lattice vectors were fixed. We employed the Perdew-Zunger exchange-correlation functional, norm-conserving pseudopotentials for all atoms, and a plane-wave basis set with a kinetic energy cutoff of 80 Rydberg. The pseudopotentials were obtained online from the pseudopotential library at the Quantum Espresso's website. In this work, the pseudopotentials of C.pz-vbc.UPF, H.pz-vbc.UPF, S.pz-bhs.UPF, and Si.pz-vbc.UPF were used for C, H, S, and Si, respectively. The electronic self-consistency was converged to  $10^{-6}$  eV, while the atoms were relaxed with a total energy tolerance of  $10^{-4}$  Rydberg, together with a

force tolerance of  $10^{-3}$  Rydberg/Bohr. The k-point mesh was set to  $10 \times 10 \times 1$ , with the  $10 \times 10$  mesh lying in the  $a^*b^*$  plane and the 1 k point along the  $c^*$  reciprocal lattice vector. A model of the TESADT film was then constructed on the basis of the optimized structure by enclosing a single molecular layer in the ab plane. The vector c was doubled from that of the bulk structure to construct a supercell, which ensures the single molecular layer is isolated from its neighboring molecular layers by  $16.5\text{\AA}$  vacuum layers (the thickness of one molecular layer). Finally, the Kohn-Sham wavefunctions for the film were generated under the same conditions as in the relaxation, to be used for subsequent UV-Vis spectroscopic calculations.

The macroscopic dielectric function was calculated using the Yambo code,<sup>2</sup> at the level of TDDFT with an ALDA approximation. The Kohn-Sham wavefunctions saved previously were used at the full 80 Rydberg cutoff. For the optical spectrum calculation, we retained a finite number of valence bands and conduction bands immediately below and above the Fermi level. We tested convergence of the optical spectrum by using window sizes ranging from (10,10) to (60,60), where the first number of each pair indicates the number of valence bands whereas the second number is for conduction bands. Local field effects were considered to account for the charge oscillations induced by the external applied potential. Dimensions of the response function and the exchange-correlation kernel were set to a size ranging from 100 up to 300. The TDDFT Dyson equation was solved in reciprocal space.

The theoretical spectrum was blue shifted by a scissor operator of  $D = 1.08$  eV to account for the underestimation of DFT bandgap.<sup>3</sup> Comparison between the

theoretical absorption spectrum and the experimental one shows that almost all of the main features are well captured by TDDFT calculations. The three absorption peaks in the range of 500-600 nm are well reproduced, although the relative intensities are slightly different from the experiment. The two low intensity peaks, located at 417 and 446 nm are slightly red-shifted compared to the experimental absorptions, but the difference is  $\leq 16$  nm. The next three peaks from 300-380 nm correspond to the rather broad experimental peak around 320 nm, which is not resolved but instead shows an apparent shoulder at the longer wavelength side. Good agreement can also be seen in the range of 200-300 nm where some intermediate intensity peaks exist. In general, the agreement between theory and experiment is rather good. Since at the TDDFT level of theory used, the electron-hole interaction was not included, it seems that the excitonic effect in the TESADT film is negligible.

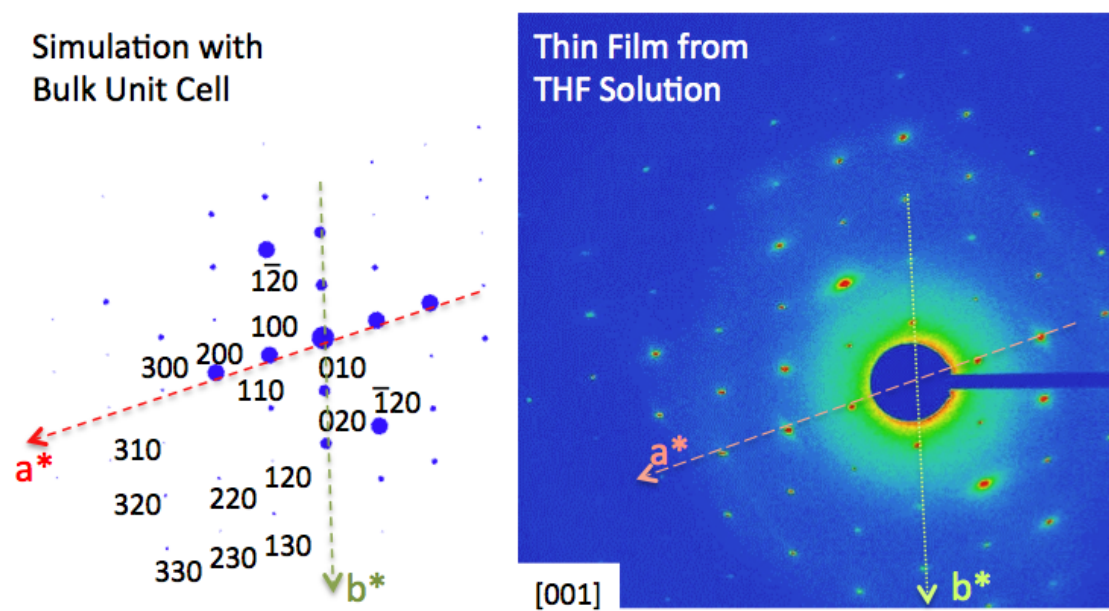


**Figure S1.** Simulated [001] zone SAED pattern of TES ADT bulk phase is compared with experimental SAED patterns obtained in TES ADT films from THF solution. The directions of  $a^*$  and  $b^*$  are marked with red and green arrows. Four additional experimental patterns are given in Figure S2, in agreement with this result.

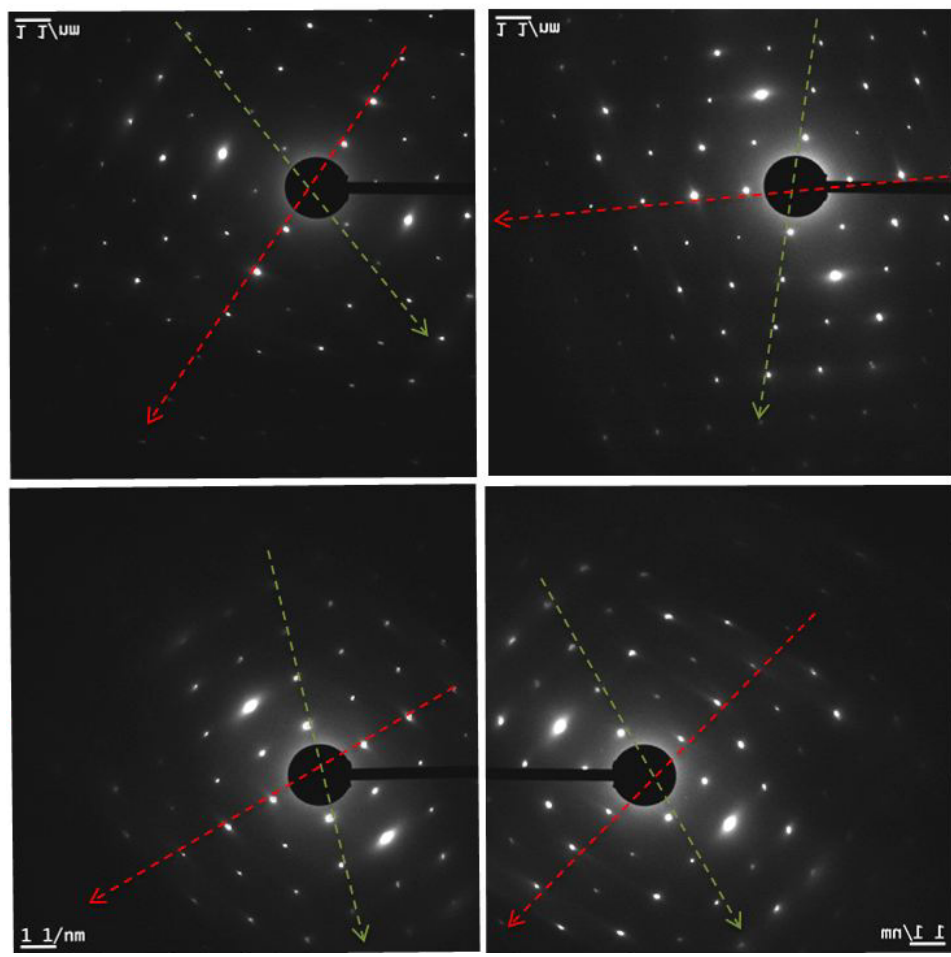


**Figure S2.** Typical [001] zone SAED patterns of TES ADT thin films crystallized from 0.2wt% THF solution by the SAC approach.

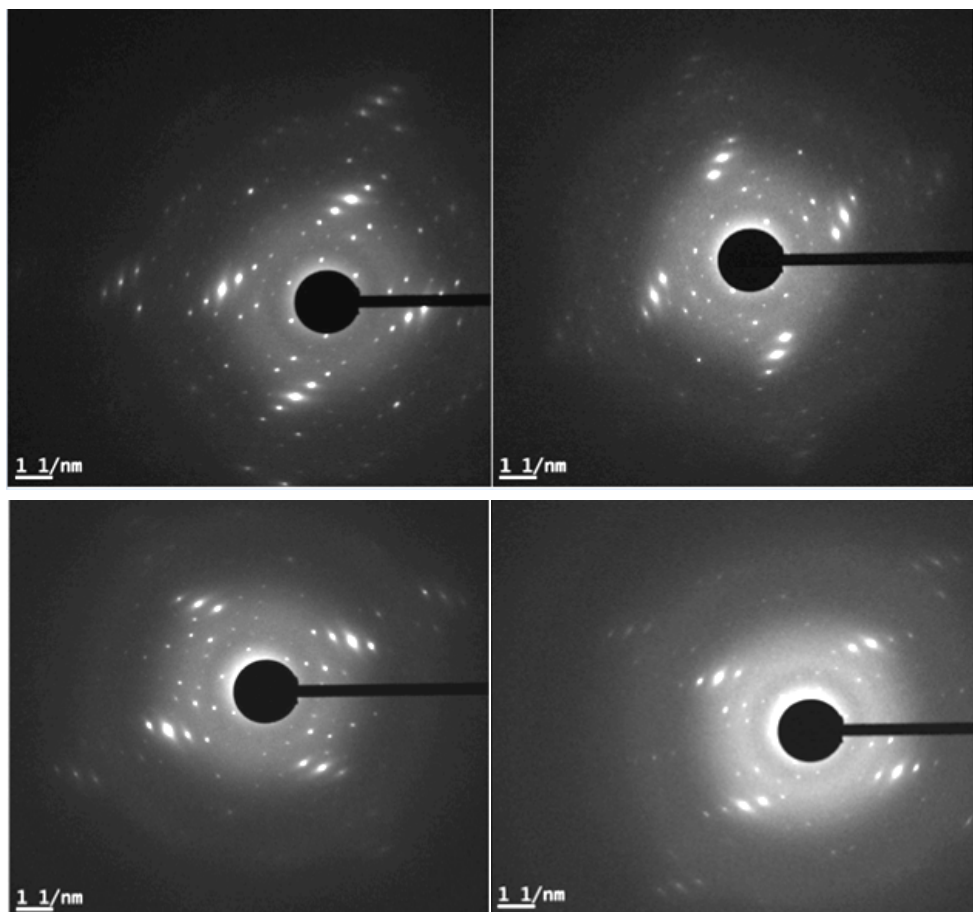


**Figure S3.** Typical [001] zone SAED patterns of TES ADT thin films crystallized from 0.2wt% toluene solution by the SAC approach. The results are consistently showing the features matched well with the so called “ $\beta$  phase” including their values of  $a^*$ ,  $b^*$  and angle  $\gamma$ .



**Figure S4.** Optical micrograph of TES ADT thin film crystallized from chloroform solution.

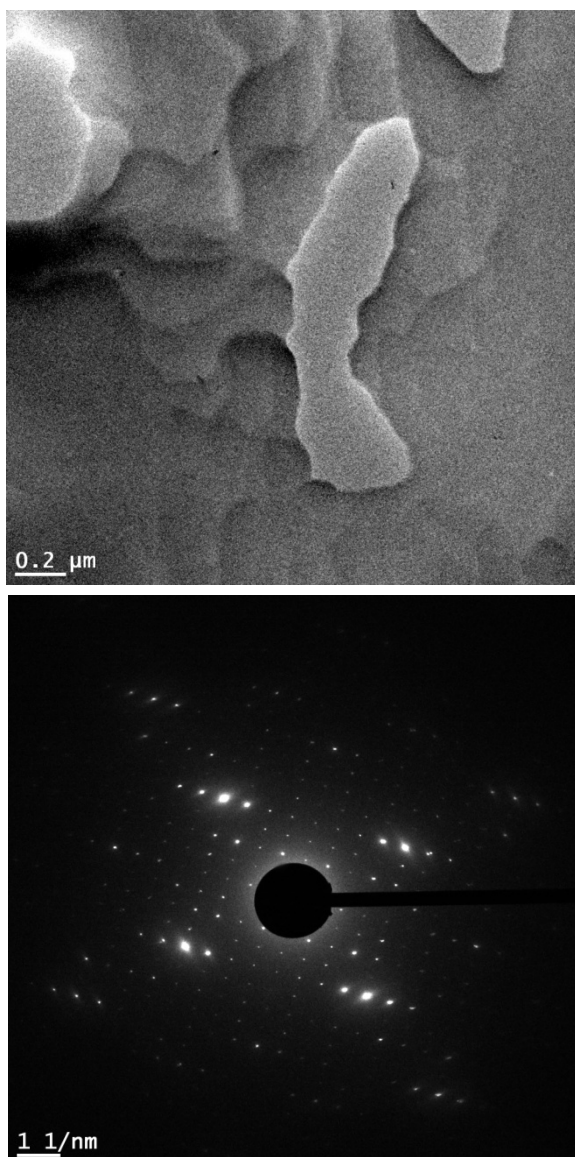


**Figure S5.** Representative bright-field TEM and SAED of TES ADT films crystallized from Hexane solution

**Reference:**

- 1 P. Giannozzi, S. Baroni, N. Bonini, M. Calandra, R. Car, C. Cavazzoni, D. Ceresoli, G. L. Chiarotti, M. Cococcioni, I. Dabo, A. Dal Corso, S. de Gironcoli, S. Fabris, G. Fratesi, R. Gebauer, U. Gerstmann, C. Gougaussis, A. Kokalj, M. Lazzeri, L. Martin-Samos, N. Marzari, F. Mauri, R. Mazzarello, S. Paolini, A. Pasquarello, L. Paulatto, C. Sbraccia, S. Scandolo, G. Sclauzero, A. P. Seitsonen, A. Smogunov, P. Umari, R. M. Wentzcovitch, *J. Phys.-Condensed Matter* **2009**, *21*.

- 2 A. Marini, C. Hogan, M. Gruening, D. Varsano, *Computer Phys. Comm.* **2009**, *180*.
- 3 D. Rocca, D. Lu, G. Galli, *J. Chem. Phys.* **2010**, *133*, 164109.